# Observation of oxygen ventilation into deep waters through targeted deployment of multiple Argo-O2 floats in the north-western Mediterranean Sea in 2013

Laurent Coppola, Louis Prieur, Isabelle Taupier-Letage, Claude Estournel, Pierre Testor, Dominique Lefèvre, Sophie Belamari, S. Lereste, Vincent Taillandier

# Observation of oxygen ventilation into deep waters through targeted deployment of multiple Argo-$O_2$ floats in the north-western Mediterranean Sea in 2013

**L. Coppola[1], L. Prieur[1], I. Taupier-Letage[2], C. Estournel[3], P. Testor[4], D. Lefevre[2], S. Belamari[5], S. LeReste[6], and V. Taillandier[1]**

[1]Sorbonne Universités, UPMC, Université Paris 06, CNRS, Laboratoire d'Océanographie de Villefranche, Villefranche-sur-Mer, France, [2]Aix-Marseille Université, CNRS/INSU, Université de Toulon, IRD, Mediterranean Institute of Oceanography, Marseille, France, [3]Université de Toulouse, CNRS, Laboratoire d'Aérologie, Toulouse, France, [4]CNRS/IRD/UPMC University Paris 06, MNHN, LOCEAN, Paris, France, [5]Météo-France, CNRS, CNRM-GAME, Toulouse, France, [6]IFREMER RDT/I2M, Brest, France

**Abstract** During the winter 2013, an intense observation and monitoring was performed in the north-western Mediterranean Sea to study deep water formation process that drives thermohaline circulation and biogeochemical processes (HYMEX SOP2 and DEWEX projects). To observe intensively and continuously the impact of deep convection on oxygen ($O_2$) ventilation, an observation strategy was based on the enhancement of the Argo-$O_2$ floats to monitor the offshore dense water formation area (DWF) in the Gulf of Lion prior to and at the end of the convective period (December 2012 to April 2013). The intense $O_2$ measurements performed through shipborne CTD casts and Argo-$O_2$ floats deployment revealed an $O_2$ inventory rapidly impacted by mixed layer (ML) deepening on the month scale. The open-sea convection in winter 2013 ventilated the deep waters from mid-February to the end of May 2013. The newly ventilated dense water volume, based on an Apparent Oxygen Utilization (AOU) threshold, was estimated to be about $1.5 \times 10^{13}$ $m^3$ during the DWF episode, increasing the deep $O_2$ concentrations from 196 to 205 $\mu mol\ kg^{-1}$ in the north-western basin.

**Correspondence to:**
L. Coppola,
coppola@obs-vlfr.fr

**Citation:**
Coppola, L., L. Prieur, I. Taupier-Letage, C. Estournel, P. Testor, D. Lefevre, S. Belamari, S. LeReste, and V. Taillandier (2017), Observation of oxygen ventilation into deep waters through targeted deployment of multiple Argo-$O_2$ floats in the north-western Mediterranean Sea in 2013, *J. Geophys. Res. Oceans*, *122*, doi:10.1002/2016JC012594.

## 1. Introduction

Open ocean deep convection is a major event in which dense waters are formed in winter in specific areas (Greenland Sea, Labrador Sea, Weddell Sea, and Mediterranean Sea). In the western Mediterranean basin, deep convection occurs during episodes of cold and dry winds (Mistrals and Tramontane). Such storm events are associated with sea surface cooling and intense evaporation. When such episodes are frequent enough, convection is deep enough to reach the sea bottom as in 1986–1987 [*Herrmann et al*., 2008; *Leaman and Schott*, 1991] and 2004–2005 [*Herrmann et al*., 2010; *López-Jurado et al*., 2005]. In contrast, when winters are not sufficiently cold, the convection is inhibited and an accumulation of heat and salt affects the intermediate waters.

To understand the impact of the convection process, it is important to emphasize that there is a hierarchy of processes and complexity in the interaction between the processes acting in the successive phases of preconditioning, convection, restratification [*Marshall and Schott*, 1999]. The latter includes the poorly known dispersion of dense water formed during each storm event, as well as the complexity of their interaction with the biogeochemical content. In the north-western Mediterranean, the preconditioning is due to isopycnal doming and cyclonic mesoscale circulation. The presence of the Northern Current (NC) and the Balearic Front (BF) to the south isolate the central part of Gulf of Lion yielding to higher sensitivity to wind forcing. When surface waters are dense enough, a vertical mixing occurs with strong vertical sinking velocities (around 10 cm $s^{-1}$). This chimney is contained in a mixed patch with eddies on its edge. When the dense waters reach the equilibrium depth, spreading phase starts.

Ventilation of the north-western Mediterranean Sea is known to be intermittent and associated with the dense water formation (DWF) rates. Recent intense deep water formation events in the western Mediterranean in 2005 produced a large amount of new WMDW (Western Mediterranean Deep Water) that has begun to modify the deep stratification of the entire basin causing abrupt increases in deep water

temperature and salinity [*Schroeder et al*., 2008b]. This event (WMT for "Western Mediterranean Transient") [*CIESM*, 2009] induced huge oxygen ventilation in the western basin [*Schneider et al*., 2014]. Previous studies estimated the dense water volume from shipborne CTD casts, density levels change in deep waters and numerical models [*Béranger et al*., 2010; *Durrieu de Madron et al*., 2013; *Herrmann et al*., 2010; *Schroeder et al*., 2010]. More recently, ventilation changes were detected in the Mediterranean Sea from long-term regular ship cruises (Med-SHIP program) and measurements of transient tracers [*Schroeder et al*., 2015; *Stöven and Tanhua*, 2014]. However, one of the major challenges in the convection and ventilation studies is to parametrize the complex 3-D of the processes involved and to estimate the newly ventilated dense water that will affect the biogeochemical contents and subsequent spring bloom. From previous studies, the amounts of newly ventilated dense water produced during deep convection events were uncertain due to observational limits. Classical research cruises are not capable enough to improve our vision of the oceanic environment during deep convection event due to its multiscale variability and the severe weather conditions that generally prevents the use of ships. Thanks to autonomous mobile platform technology (Argo floats, gliders) and the accuracy of the data produced, a better description of convection mechanism is now possible. This issue motivated a multiplatforms approach (ship cruises and mobile autonomous platforms) based on continuous monitoring along the water column at the multiscales over a year (P. Testor, personal communication, 2016).

During the period 2012–2013, a high-resolution physical and biogeochemical sampling covering the whole north-western Mediterranean Sea was performed during the HyMeX Special Observation Period 2 (SOP2) and the DEWEX (February and April 2013) [*Conan*, 2013; *Testor*, 2013] and MOOSE-GE cruises (July–August 2012 and June–July 2013) [*Testor et al*., 2012, 2013]. The objectives were to improve our knowledge of the vertical and horizontal processes involved during the deep convection, deep water spreading, and its interactions on biogeochemical content using the recent improvements in observation capabilities. In this paper, a description of intense measurements performed by Argo-$O_2$ floats in the DWF zone is presented and impacts of the mixed layer deepening on the $O_2$ content are discussed. Apparent Oxygen Utilization (AOU) was calculated to estimate the $O_2$ used by biochemical processes relative to its solubility value and may be more informative regarding the age of the water mass. AOU was used here as a tracer to estimate the volume of ventilated dense water in order to discuss the nature of the newly formed dense water mass and its role on the deep $O_2$ ventilation.

## 2. Materials and Methods

### 2.1. Argo-$O_2$ Floats Deployment Strategy

The observation strategy relies on the enhancement of the Argo-$O_2$ floats deployment to monitor the offshore DWF zone in the Gulf of Lion, where the deep convection process is known to occur [*Durrieu de Madron et al*., 2013; *Herrmann et al*., 2008]. To perform an effective observation of the deep convection process, four Argo-$O_2$ floats were deployed (Figure 1a): two during the preconditioning phase (late November 2012) in the northwest side of the DWF area and two in the core of the expected mixed patch (42°N5°E, late January 2013) during the active convection phase which started in mid-January 2013 (as observed by satellite and gliders) [*Bosse et al*., 2016].

The floats are based on a PROVOR CTS3, with a standard CTD sensor, equipped with an oxygen optode with fast time response (Aanderaa 4330) to measure accurately $O_2$ concentration which is here considered as a good proxy for quantifying and tracking the newly formed water masses during the convection process. Following the Argo oxygen protocol [*Thierry et al*., 2016], the Aanderaa optodes 4330 were sent to the CSIRO facilities for a more robust calibration [*Uchida et al*., 2008]. In addition, these optodes were cross-validated in laboratory before deployment and also during the floats deployment by colocated CTD profiles and water samples (Niskin bottles). The four PROVOR floats were also equipped with an iridium antenna to ensure a two-way communication. It allowed us to shift the Argo floats cycle during their deployment going from a 5 day cycle (0–2000 m depth) before and after the convection process to a daily cycle during the convection period (data available on GDAC CORIOLIS) [*Argo*, 2000].

### 2.2. Ship Cruises

Each summer since 2010, a MOOSE-GE cruise takes place in the north-western basin to monitor water masses properties change after the winter convection process and their effects on biogeochemical cycles.

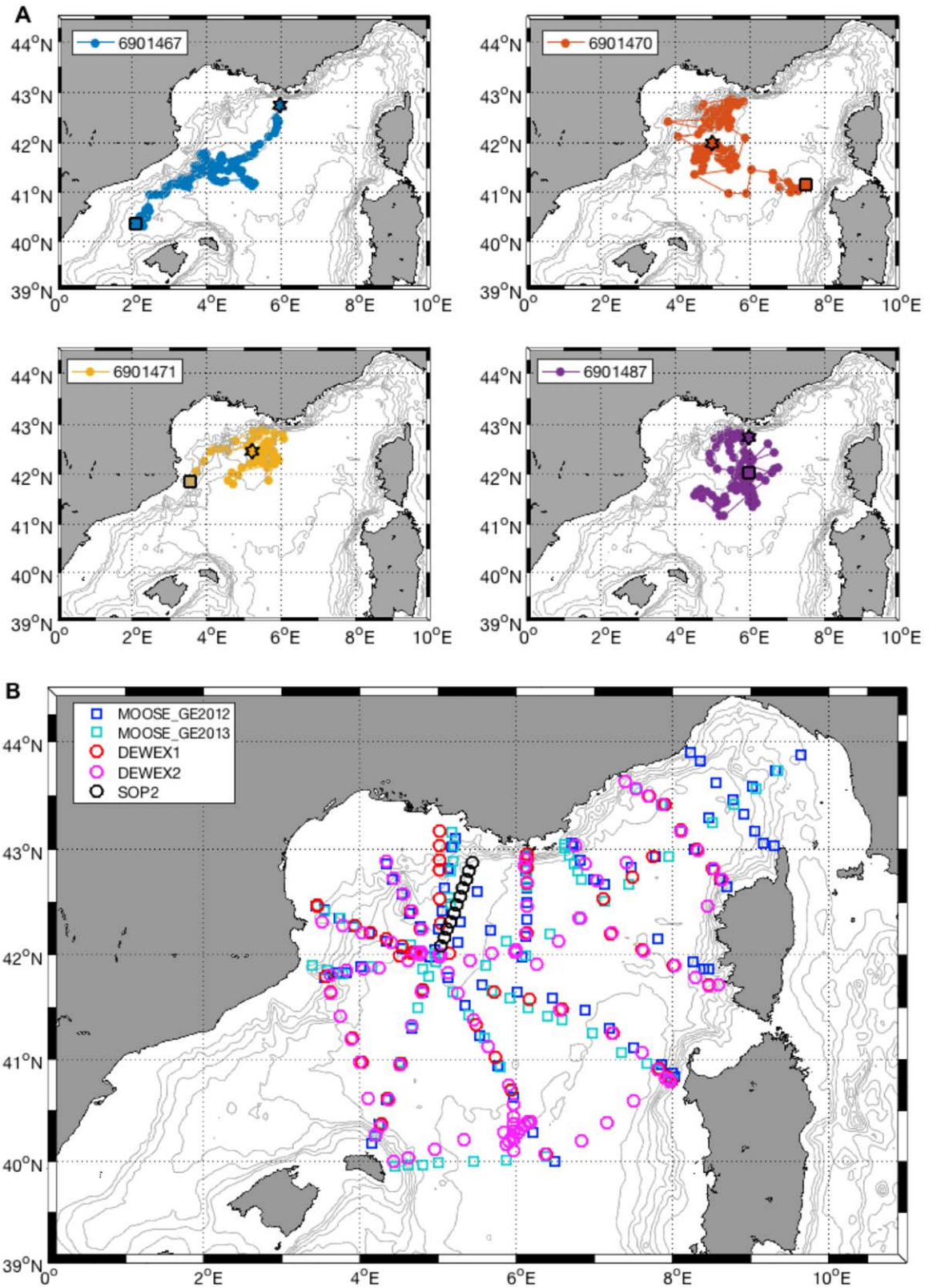


**Figure 1.** (a) Map of Argo-$O_2$ floats trajectories in the northwestern Mediterranean basin from the December 2012 to July 2013. The number represents the WMO float identifier. Floats 6901467 and 6901487 have been deployed in December 2012 and floats 6901470 and 6901471 in the end of January 2013. The black star represents the initial position and the black square the position in July 2013. (b) Ship cruises stations performed during the SOP2 cruise (January 2013), the DEWEX cruises (DEWEX1 in February 2013 and DEWEX2 in April 2013) and during the MOOSE-GE cruises in summer 2012 and 2013.

These cruises provide a yearly snapshot in summer of the open ocean part of the basin with about 70–100 $CTDO_2$ casts distributed along north-south sections and passing through the DWF area (Gulf of Lions). During the period 2012–2013, the MOOSE-GE cruises were conducted in July–August 2012 on board R/V Le Suroit (89 stations) and in June–July 2013 on board R/V Téthys II (72 stations) (Figure 1b).

Following a similar strategy, the DEWEX cruises, which took place between the summer cruises (in February and April 2013), provided data on the hydrological conditions prior, during and after the winter convection in early 2013 (Figure 1b). The objective of DEWEX was to study the role played by the formation of deep water in the chemical composition and budgets of organic matter in the Mediterranean Sea and to understand the relationships between the plankton food webs and the hydrodynamic structures (related to MerMEX project). In addition, cruises dedicated to support the HyMeX SOP2 operations were set up in late January 2013 and used to deploy the Argo-$O_2$ floats near the DWF zone with 11 CTD casts operated onboard R/V Téthys II [*Taupier-Letage and Bachelier*, 2013].

### 2.3. Data Quality Control Procedures

Pressure, temperature (T), conductivity (C), and dissolved oxygen (DO) measurements during the MOOSE-GE and DEWEX cruises were made using a Seabird SBE 911+ CTD probe and SBE43 sensor. The CT and DO sensors were calibrated before the cruises operation and after with postcruises manufacturer calibrations (V. Taillandier, personal communication, 2016). After calibration, the accuracy of the measurements given by manufacturer is 0.001°C for the temperature, 0.003 for the salinity and 2% of $O_2$ saturation (equivalent to 4 $\mu$mol $kg^{-1}$). In addition, Winkler titrations were performed on board after seawater sampling. The measurements were done each day (every 4–5 stations) and the SBE43 sensor was cleaned after each CTD-Rosette casts following the manufacturer recommendations. Later on, the Winkler analysis was used to adjust the SBE43 raw data, as specified by the GO-SHIP group (http://www.go-ship.org/).

After the Argo-$O_2$ floats deployment, CTD casts were performed as a reference measurement using the same type of CTD-Rosette than those used during MOOSE-GE and DEWEX cruises (Figure 2). Winkler analysis was complete for each cast to ensure a SBE43 data adjustment. Intercomparison between $CTDO_2$-ship and $CTDO_2$ floats profiles provided an offset at the start of the floats deployment. A second intercomparison was done for all floats using the MOOSE-GE and DEWEX stations located close enough to the Argo floats positions (distance $<$ 10 km) and with the shortest time delay available (Figure 2). It offers the opportunity to evaluate an offset and a drift existing on sensors mounted on Argo floats [*Takeshita et al*., 2013]. For the Argo float 6901487, the larger time difference between shipborne $O_2$ profile and Argo-$O_2$ profile did not change the good similarity between both profiles and indicates that $O_2$ correction is still suitable. Finally, both procedures (at deployments and 5–6 months later) provide final drifts and offsets for T, S, and $O_2$ which were used to adjust the Argo floats profiles during their life cycle (Table 1). The drifts for T, S, and $O_2$ are negligible for the all data sets. Despite this delayed mode adjustment, the float 6901487 provided bad salinity data at deep waters (below 500 m), probably due to technical issues on the conductivity sensor. These salinity data were removed from our study.

### 2.4. Argo-$O_2$ Floats Data Set

The activity of the four Argo floats was based on different life cycle settings and was also affected by individual battery capacity and technical issues encountered. During the HYMEX SOP2, floats 6901467 and 6901487 circulated during 12 cycles with a time scale of 5 days before switching to a daily cycle for 93 cycles (mid-January to end of April) and then switched back to 5 days' cycle. The floats 6901470 and 6901471 started with a daily cycle for 88 cycles (February to end of April) and then switched to 5 days' cycle. In total, each Argo float performed between 111 and 204 cycles (or vertical profiles).

The final offsets for T, S, and $O_2$ sensors were estimated. For T and S data, offsets ranged from $-0.02$ to 0.01°C and from $-0.005$ to 0.009, respectively, except for float 6901487 that showed bad salinity data at depth. T and S offsets are respectively 10 and 3–4 times higher than nominal accuracy ($\pm$0.002 for T and S) proposed by sensors manufacturer (SBE41 from SeaBirdElectronics). For all Argo floats, optode offset ranged from 22 to 28 $\mu$mol $kg^{-1}$ (Figure 2). This offset is larger than the Aanderaa sensor specificity (accuracy $<$ 8 $\mu$mol $kg^{-1}$) and probably due to bad storage conditions. However, predeployment and postdeployment intercomparisons suggest that such offsets remained constant during the life of Argo floats (gain or slope close to 1) and the delayed mode optode adjustment offered an $O_2$ resolution around 1 $\mu$mol $kg^{-1}$ which is

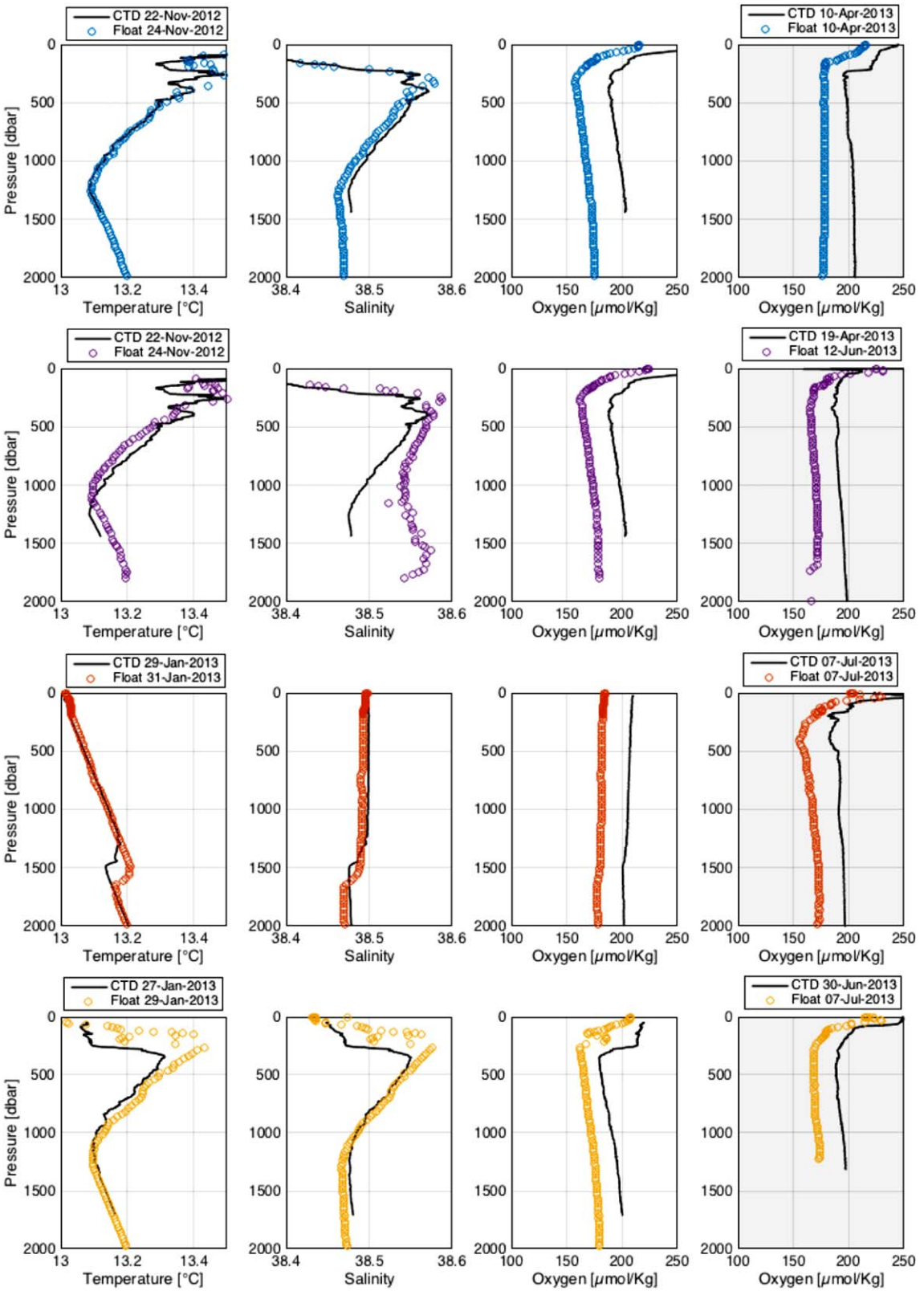


**Figure 2.** (left) Intercomparison between ship-based CTD and Argo floats profiles (in situ temperature, salinity, and dissolved oxygen) at the deployment and (right) during the life cycle of the Argo floats performed 5–6 months later during the DEWEX and MOOSE-GE cruises. All Argo floats profiles are raw data using manufacturer calibration coefficients. The colors of profiles represented the different Argo floats (blue: 6901467, purple: 6901487, red: 6901470, and yellow: 6901471).

**Table 1.** Final Offsets Applied on Argo-$O_2$ Floats to Adjust the T, S, and $O_2$ Variables

| Parameter | 6901467 | 6901470 | 6901471 | 6901487 |
|---|---|---|---|---|
| Deployment date | 11/22/2012 | 01/29/2013 | 01/27/2013 | 11/22/2012 |
| Total cycles | 204 | 164 | 111 | 157 |
| T offset (°C) | 0.011 | 0.011 | −0.023 | −0.025 |
| S offset | 0.008 | 0.009 | −0.005 | −0.071[a] |
| $O_2$ offset (μmol $kg^{-1}$) | 28.2 | 23.0 | 22.0 | 23.5 |

[a]For the Argo float 6901487, the salinity below 1000 m has a bad QF code and has been removed for the study.

accurate enough to provide a robust $O_2$ data set [*Takeshita et al.*, 2013; *Thierry et al.*, 2016; *Uchida et al.*, 2008].

### 2.5. Mixed Layer Depth Estimation

The mixed layer (ML) depth was estimated based on potential density profiles ($\sigma$), calculated from P, T, and S data corrected from the sensors offsets (see section 2.3). For each potential density profile, the ML depth corresponds to the depth where the difference between the potential density at the reference depth (10 dbar) and the measured potential density is higher than the threshold of 0.01 kg $m^{-3}$. During deep convection event, a potential density threshold of 0.01 kg $m^{-3}$ is more appropriate to better represent the vertical mixing in winter in the Gulf of Lion due to its weak stratification [*Houpert et al.*, 2016; *Loveday et al.*, 2012]. When a profile is found to be completely homogeneous ($\Delta\sigma < 0.01$ kg $m^{-3}$), according to this criterion, the ML depth is associated with the maximal depth of the profile (i.e., 2000 m).

### 2.6. AOU and Ventilated Dense Water Volume Calculation

The volume formed by the deep ventilation during the winter 2013 was based on AOU threshold representative of recently formed dense waters (<48 μmol $kg^{-1}$) where potential density was higher than 29.11 kg $m^{-3}$ (supporting information Figure S2). AOU was calculated as the difference between $O_2$ gas solubility and the measured $O_2$ concentrations. The $O_2$ solubility was calculated as a function of in situ temperature and salinity, and one atmosphere of total pressure. It was determined with the equation of Garcia and Gordon [*Garcia and Gordon*, 1992] and coefficients of Benson and Krause [*Benson and Krause*, 1984]. AOU gives a temporal integration of all processes that influence $O_2$ content, i.e., production and removal toward atmosphere and lateral mixing. Oxygen production is confined to surface waters where photosynthesis and atmospheric $O_2$ inputs occur. Oxygen consumption takes place during remineralization processes in the ocean interior. Using AOU estimate represents the amount of $O_2$ that was removed. Consequently, younger surface water mass is associated with lower AOU, opposite to deep and old water mass supplied by neither photosynthesis nor by $O_2$ ventilation [*Ito et al.*, 2004]. Using AOU to estimate the volume of new dense water formation requires intense and accurate measurements of $O_2$ concentrations during the deep convection process. Such a methodology can be applied here thanks to the intensive Argo-$O_2$ floats deployment, with daily data acquisition and data adjustment operated in this study.

In the present study, the ventilated dense water volume corresponds to the dense water mass recently formed and oxygenated (due to $O_2$ atmospheric supply) related to rapid transport from surface to deep waters during the intense vertical mixing. In this paper, in situ data (ships and Argo floats) were used during the DWF period (from January to April 2013) to determine the minimum depth of the dense water mass within the AOU threshold (<48 μmol $kg^{-1}$) and a potential density higher than 29.11 kg $m^{-3}$ (typical value for the newly formed dense waters in the north-western Mediterranean Sea) [*Durrieu de Madron et al.*, 2013]. Consequently, when part of profiles satisfied concomitantly both thresholds, new ventilated dense water was assumed sampled. The corresponding depth represents the minimum depth of the new ventilated dense water. Then, this minimum depth was interpolated with Delaunay triangulation method to establish a surface corresponding to the upper depth boundary of the new ventilated dense water. Finally, assuming that the new ventilated dense water reaches the seafloor, the volume of this water mass extends from the interpolated upper boundary surface to the bottom depth corresponds to the volume of the new ventilated dense water.

## 3. Results and Discussion

### 3.1. Argo-$O_2$ Floats Profiles and Trajectories

During the DWF period (January–April 2013), in situ observation was intense with 345 Argo-$O_2$ profiles (0–2000 m) corresponding to three profiles per day (in comparison ship cruises performed 77 profiles from

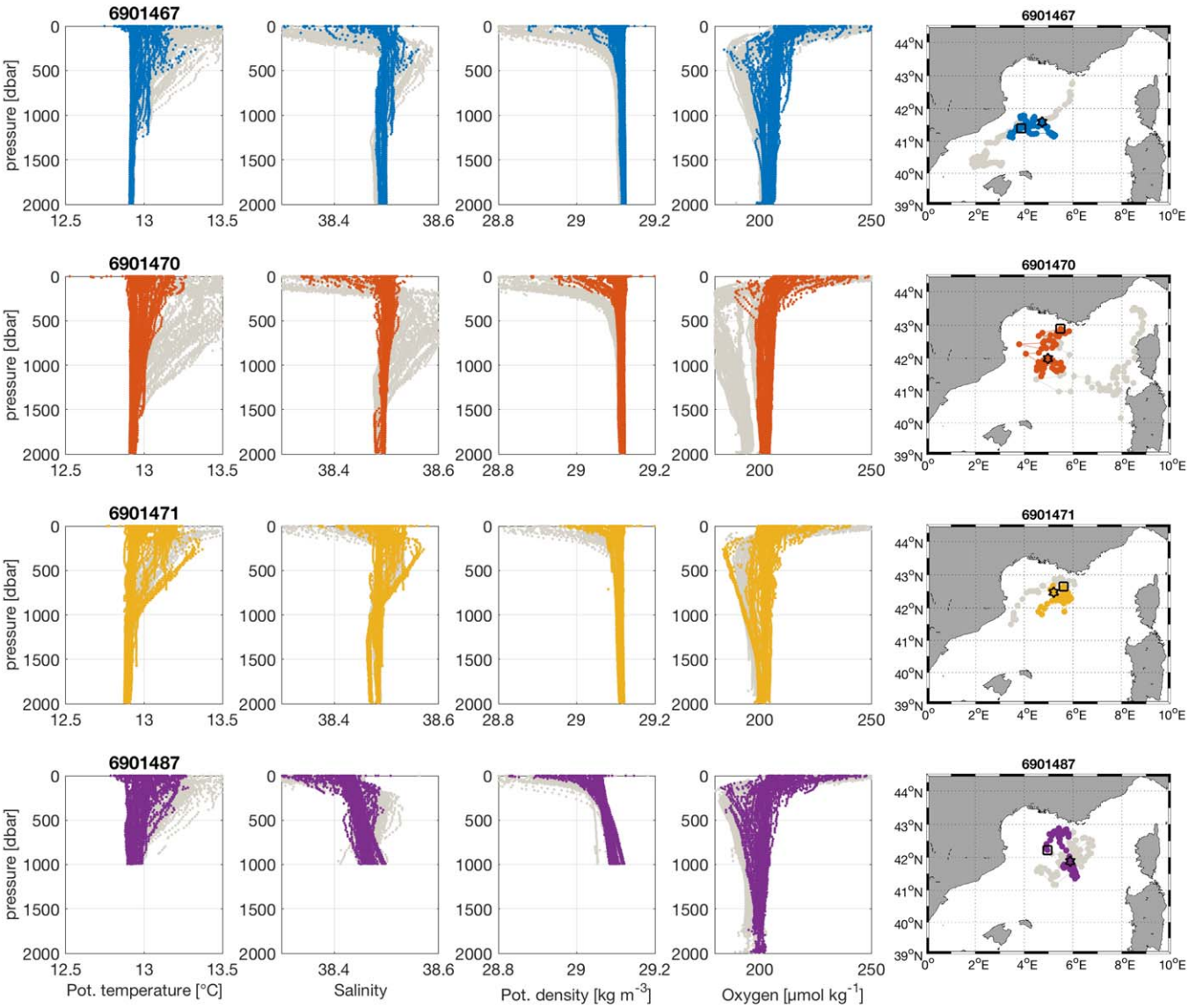


**Figure 3.** Argo floats adjusted profiles and positions (potential temperature, salinity, potential density, and dissolved oxygen) during their deployment. The colors represent the data for each Argo floats during the intense mixing period (February–March 2013). The grey color represents the all data set. For the float 6901487, salinity below 1000 m have been removed (sensor issue). The black star represents the initial position and the black square the final position during the DWF process (i.e., 1 February and 30 March, respectively).

surface to near bottom depth during the same period). In particular, during the convection process (February–March 2013) two sorts of drifting behavior were observed (Figure 3): two quasi-stationary floats (6901471 and 6901487) were located inside the mixed patch, while the other two floats (6901467 and 6901470) moved to the south west near the Balearic Islands and to the south-east near Sardinia, respectively. The quasi-stationary floats observed deep mixing for longer time than the ones that exited the DWF zone before the end of the convection process (Figures 3 and 4). During the intense mixing period (February–March 2013), the potential temperature and salinity vertical profiles from the four Argo floats are in the same range: from 12.50 to 13.55°C and 38.20 to 38.65, respectively. During the same period, potential density ranged from 28.85 to 29.12 kg $m^{-3}$ and $O_2$ from 190 to 250 µmol $kg^{-1}$. Otherwise, after the DWF period and outside the mixed patch, those variables presented a wider range: 12.8–25.9°C, 37–38.6, 28–29.12 kg $m^{-3}$, and 170–290 µmol $kg^{-1}$ for potential temperature, salinity, potential density, and dissolved oxygen, respectively (not shown).

After intense atmospheric forcing events that trigger deep convection in the center of the north-western basin, a mixed patch appeared. This patch was characterized by homogenous T, S, and $O_2$ profiles with

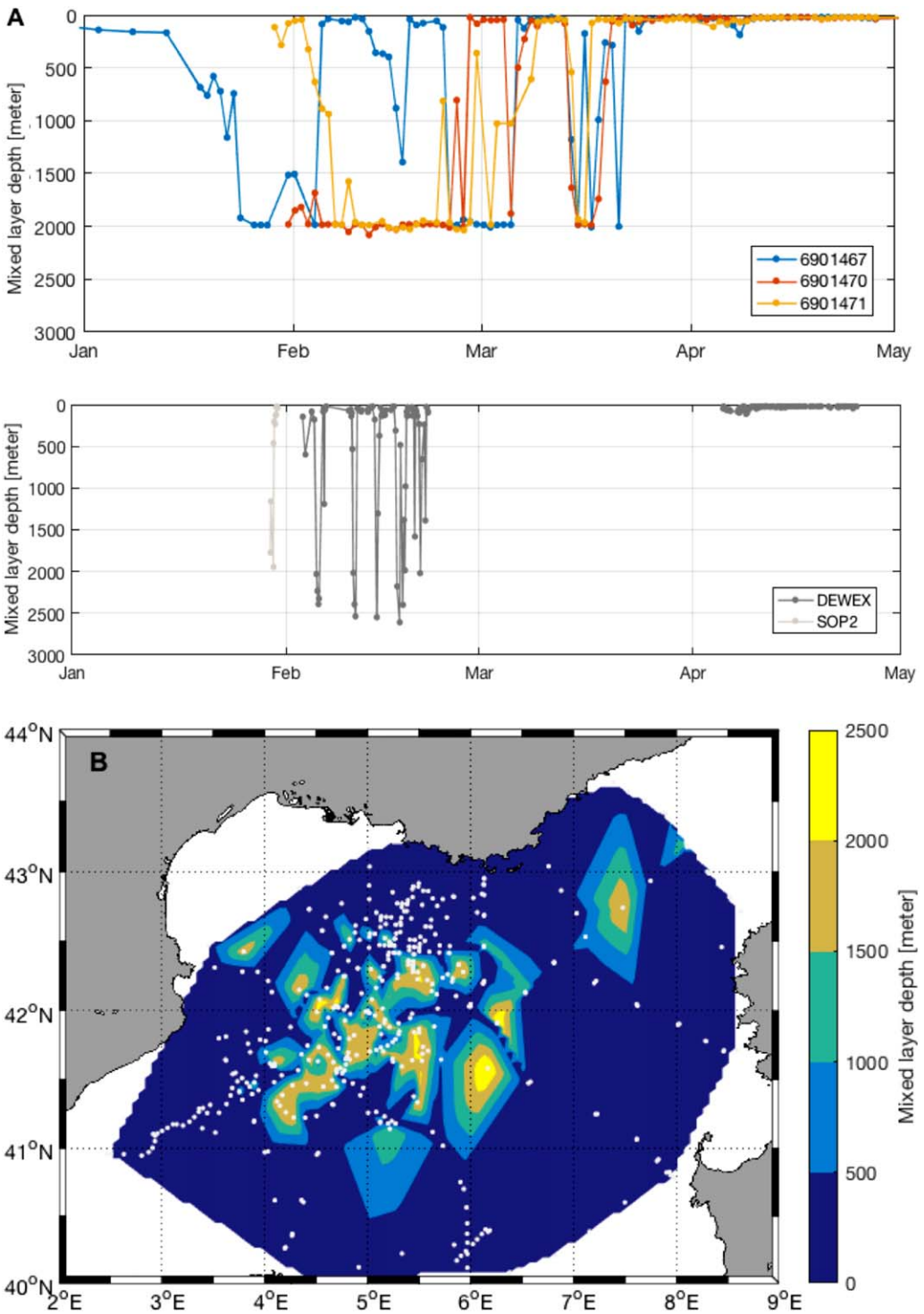


**Figure 4.** (a) (top) Mixed layer (ML) depth time series observed from January to May by Argo floats using the criterion of potential density 0.01 kg $m^{-3}$. The deepest ML is limited by the Argo float capability (2000 dbar). (bottom) ML depth estimated for DEWEX and SOP2 cruises using the same criterion for the same period. (b) Spatial variability of the ML depth merged with Argo floats and DEWEX/SOP2 cruises from January to May 2013. The grey dots represent the cast positions used to estimate the ML depth values.

reduction or absence of LIW (Levantine Intermediate Water) signal (associated with S maximum and $O_2$ minimum). This mixed patch was well represented by *Estournel et al.* [2016] who used surface chlorophyll concentrations and sea surface density to delimit the size and the timing of the mixed patch. From late January to early April 2013, this mixed patch was localized in the area within 41°N–42°N, 4°E–9°E (Figure 4b).

The trajectories of Argo floats are very heterogeneous. In effect, individual trajectories depend on the sampling time scale (cycle duration) operated by the floats: the shorter the time scale is, the more the float trajectory reveals fine circulation structures [*Taillandier et al*., 2006]. The trajectory of float 6901467 deployed near the ANTARES site (42.75°N, 6°E) followed very closely the Northern Current (NC), especially during the 5 day cycle starting on 11 November 2012 (Figures 1 and 3, maps on right). When the float switched to daily cycle, the float was captured inside the DWF zone and exited the area in mid-March 2013. From this date, it followed the course of NC then was confined in the Balearic Islands vicinity from July 2013 until the end of its life cycle (June 2014). For the float 6901487, the deployment strategy was identical but it was captured rapidly in small scale structures resulting in looping trajectories [*Taillandier et al*., 2006]. Argo floats 6901470 and 6901471 were deployed at the end of January, inside the mixed patch, with daily time sampling until the end of April. Consequently, the presence of submesoscale eddies (5–10 km) in the DWF zone during winter [*Testor and Gascard*, 2006] resulted in looping trajectories, positioned inside the mixed patch (Figures 1 and 3). After April, the sampling time scale switched to 5 days and the floats followed the NC path (6901471) or the LIW branch and the Western Corsica Current (6901470) [*Bosse et al*., 2015; *Millot and Taupier-Letage*, 2005].

### 3.2. Temporal Evolution of the Mixed Layer Deepening and Oxygen Ventilation

In the Gulf of Lion, the Mistral and Tramontane (northerly and north-westerly wind, respectively) frequently affect this area. Associated with the basin-scale cyclonic circulation, which drives a doming of isopycnals, these strong winds induce in winter an intense surface buoyancy loss that triggers the deepening of the mixed layer. From atmospheric and oceanic model simulations applied in the DWF area during the HYMEX-SOP2, the winds chronology affecting the production of dense water showed strong northely winds ($>$15 m $s^{-1}$) from mid-January 2013 followed by a first peak in 2–8 February 2013 ($\sim$23 m $s^{-1}$, direction NW) associated with a strong Mistral event, a second peak in 23–26 February 2013 ($\sim$17 m $s^{-1}$, direction WNW) and a third peak in 13–15 March 2013 (21–23 m $s^{-1}$, direction NW) [*Léger et al*., 2016] (supporting information Figure S1).

The ML depth estimated from Argo floats ranged from 10 to 2000 m (Figure 4a). ML depth results suggest that dense water formation was first observed in 25 January 2013 by float 6901467. In the subsequent period, the three floats (6901467, 6901470, and 6901471) continuously observed ML depth at about 2000 m (until 5–8 March), with some secondary late deep convection in mid-March. However, Argo floats pressure capacity limits bottom waters sampling (below 2000 m) and introduces a bias in the maximum ML depth observable by floats. Indeed, ML down to 2500 m (close to the seafloor) has been observed in February 2013 through shipborne CTD casts during DEWEX cruise LEG1 (Figure 4a). Then, we can consider that high ML depth estimated from the Argo floats was close to the seafloor, which ranges from 2300 m in the center to 2500 m in the south of the mixed patch.

Considering all observations available (Argo floats and shipborne CTD casts), the depth and coverage of the ML are very heterogeneous (Figure 4b). During the DWF period, the largest mixed patch was observed in the center and in the west of the northwestern basin, limited in the north by the NC and in the south by the BF. A second mixed patch was observed in the Ligurian Sea and the deepest ML was located at 90–110 km from the coast based on shipborne CTD casts and glider sections [*Bosse et al*., 2016]. This observation is consistent with high-resolution oceanic simulations of ML depth performed during HYMEX SOP2 operation [*Léger et al*., 2016].

In general, it is known that the ML deepening influences strongly the oxygen supply, especially during intense open-sea convection [*Frob et al*., 2016; *Kortzinger et al*., 2004]. To describe such process, we estimated an $O_2$ inventory (or content in mol $m^{-2}$) corresponding to the integration of $O_2$ concentrations from surface to 2000 m by using trapezoidal method. The time series of the $O_2$ inventory observed by the 3 Argo floats (6901467, 6901470, and 6901471) are different and reflect their singular trajectories inside or outside the mixed patch (Figure 5a). The float 6901467 was more confined in the south-west of the mixed patch while the float 6901470 explored the north-east in February then, the south part of the mixed patch in late April. Finally, the float 6901471 observed the east and north-east part of the mixed patch (Figure 5a). Inside the mixed patch, the $O_2$ content shows an increase from 395 mol $m^{-2}$ in January 2013 to 420 mol $m^{-2}$ in March 2013 (Figure 5b). Outside the patch, the $O_2$ content ranged around 385–390 mol $m^{-2}$. The increase of $O_2$ content in the DWF zone is higher and faster than that observed in the Labrador Sea (17 mol $m^{-2}$ in

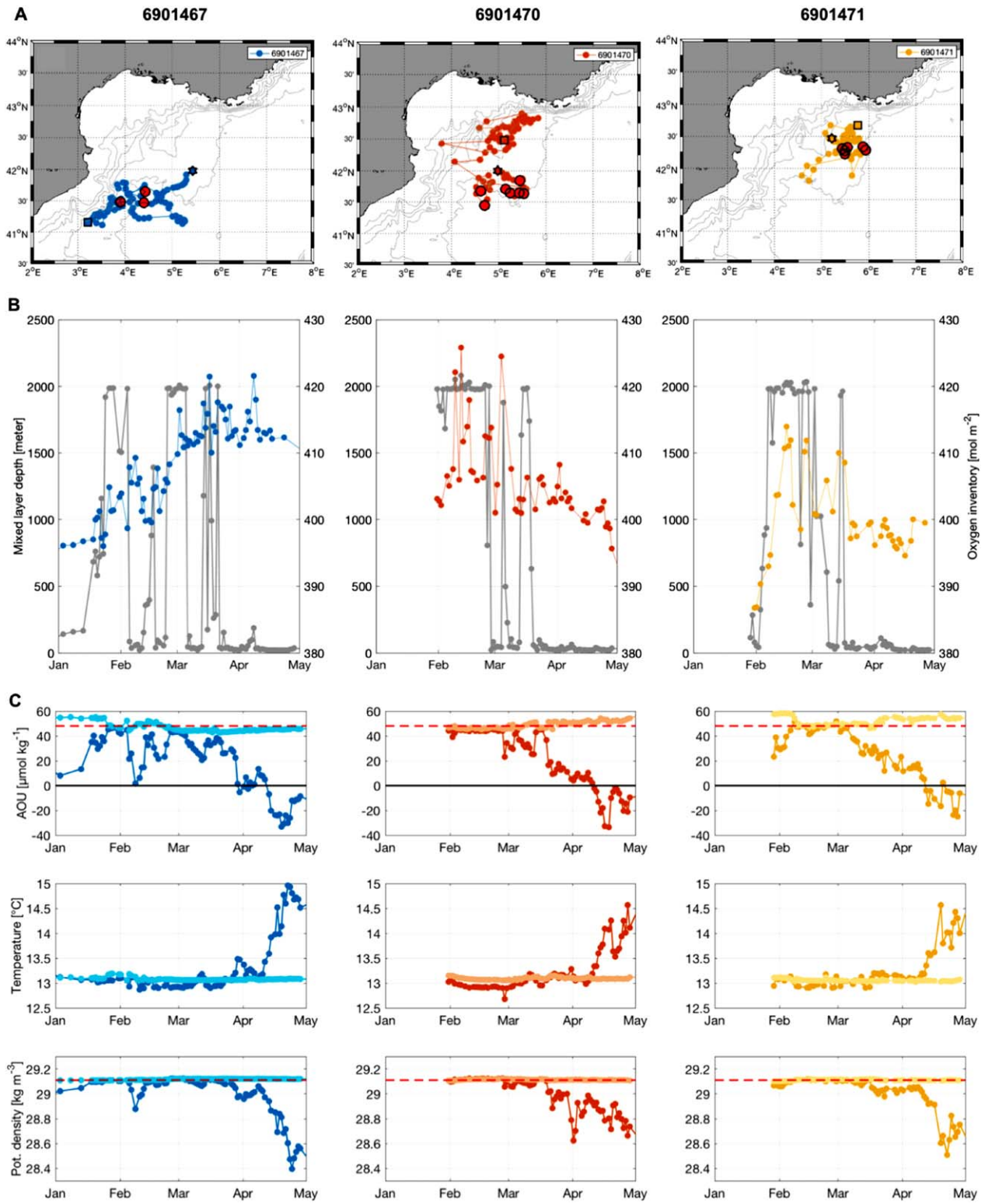


**Figure 5.** (a) Argo floats trajectories during the ML deepening. The black star and the black squares represent the floats position in 8 January 2013 and 14 April 2013, respectively. The red circles correspond to the floats position when ML depth was close to 2000 m. The contour lines represent the bathymetry levels every 500 m. (b) Oxygen dynamic during the open-sea deep convection in period January–May 2013. The values correspond to the oxygen inventory (mol $m^{-2}$) integrated from surface to 2000 m (color dots and lines) during the ML deepening (grey line) observed by the Argo floats (6901467, 6901470, and 6901471). (c) From the top to the bottom: time series of Apparent Oxygen Utilization (AOU), in situ temperature, and potential density for floats 6901467 (blue), 6901470 (red), and 6901487 (yellow) at 10 and 1000 m depth (respectively in dark and lighter color). The dashed lines in the top and bottom represent the AOU and potential density thresholds (48 µmol $kg^{-1}$ and 29.11 kg $m^{-3}$, respectively).

2.5 months) by *Kortzinger et al*. [2004] possibly because the ML is deeper in the Gulf of Lion. In the Labrador Sea, during the open convection, the ML depth generally reaches 1000–1400 m whereas in the Gulf of Lion, the ML depth can reach the seafloor based on long time series (LION mooring) [*Houpert et al*., 2016]. This emphasizes the intensity of such hydrodynamic process in this area and its capacity to renew the entire water column, which is unique in the Mediterranean Sea.

The predominant mechanisms which may explain such an intense $O_2$ intake are the air-sea fluxes and the deepening of the ML. In January–February, when both processes are active in the north-western Mediterranean Sea, large volumes of undersaturated water are exposed to the atmosphere, leading to a strong $O_2$ ingassing. During the intense vertical mixing, the $O_2$ supply invaded the water column and the $O_2$ content increased. This event is well observed in February by floats 6901470 and 6901471 for ML depth at about 2000 m, AOU (20–48 $\mu$mol $kg^{-1}$), temperature (13–13.2°C), and density (around 29.11 kg $m^{-3}$) values between surface (10 m) and deep waters (1000 m) shown in Figure 5c. For the float 6901467, its passage inside and outside the mixed patch impacted the $O_2$ inventory signal and the increase of $O_2$ content appeared slower (Figure 5b). Indeed, during the same period, this float showed AOU with a wider range (0–48 $\mu$mol $kg^{-1}$), which is consistent to its passage through unmixed water masses (Figure 5c).

After the last deep convection event (i.e., mid-March) [*Léger et al*., 2016], $O_2$ content decreased rapidly (Figure 5b), especially for the quasi-stationary floats (6901470 and 6901471). This observation could be explained by the vertical spreading of the newly formed dense water to deeper layers, leading to a lateral intrusion of less oxygenated LIW. From early April, sea surface temperature (SST) increased while density decreased and lower AOU appeared (Figure 5c). During this period, shallower mixed layer (less than 100 m) and higher SST constitute adequate condition to the start of phytoplankton blooming, yielding a production of $O_2$ by photosynthetic processes [*Mayot et al*., 2017]. At the same time, the surface water warming balanced the biological production of $O_2$ by inducing sea-to-air outgassing (solubility pump) which result to a decrease in $O_2$ content. Finally, AOU concentrations in surface waters is close to zero implying that in early April, surface water $O_2$ concentrations were in equilibrium with the atmosphere (Figure 5c). From mid-April, SST increased faster and an intense bloom occurred, leading to higher $O_2$ production in surface waters and negative AOU values appeared (Figure 5c). In early May, the bloom is finished, the vertical stratification is higher and the input of nutrient-rich deep waters to euphotic layer is reduced, lowering the biologically mediated $O_2$ production: AOU values are less negative (Figure 5c). At this stage, the intrusion of LIW is no longer balanced by $O_2$ production: $O_2$ content reached is minimum level (around 380 mol $m^{-2}$) [*Copin-Montégut and Bégovic*, 2002]. For the float 6901467, the $O_2$ content decrease is slightly reduced, probably due to its pathway crossing mixed and nonmixed patches. At the end of April, its location in the southwest of the DWF zone could alter the $O_2$ content signal, making its comparison with the others floats difficult.

### 3.3. Estimation of the Newly Ventilated Dense Water Volume

Dense water volume formation is usually estimated using the surface of the mixed patch (from Chl *a* concentrations at the sea surface or altimetry anomalies) integrated with ML depth (from in situ or simulated results) [*D'Ortenzio et al*., 2005; *Durrieu de Madron et al*., 2013]. Salinity budgets [*Bethoux*, 1980] and hydrology anomalies [*Schroeder et al*., 2008a] have been also used to quantify dense water volume. Deep convection has been estimated with tracers such as chlorofluoromethane and tritium concentrations [*Rhein*, 1995] and $O_2$ anomaly [*Kortzinger et al*., 2004] as proxies of ventilated intermediate and deep waters that were eroded by DWF. In the present study, we propose a new approach based on AOU concentrations which provide information on changing circulation not revealed in measurements of physical properties, such as temperature and salinity. Indeed, the AOU contains information about the age of the water parcel since in the deep ocean there are no sources of $O_2$. During deep convection event, very weak vertical gradients of temperature and salinity inside the mixed patch minimize the impact of dense water formation on water column structure. Such ambiguities may be removed by combining AOU and potential density values since ventilation process can be detected when low AOU on high isopycnals (i.e., newly formed dense water) is observed.

As the AOU variable emphasis the recent character in the newly formed dense water driven by the $O_2$ supply, in the following discussion, we rather use the expression of new ventilated dense water.

The AOU concentrations observed in deep waters in the north-western Mediterranean Sea (WMDW) changed over the seasons and showed a strong interannual variability in 2012–2013. From shipborne CTD

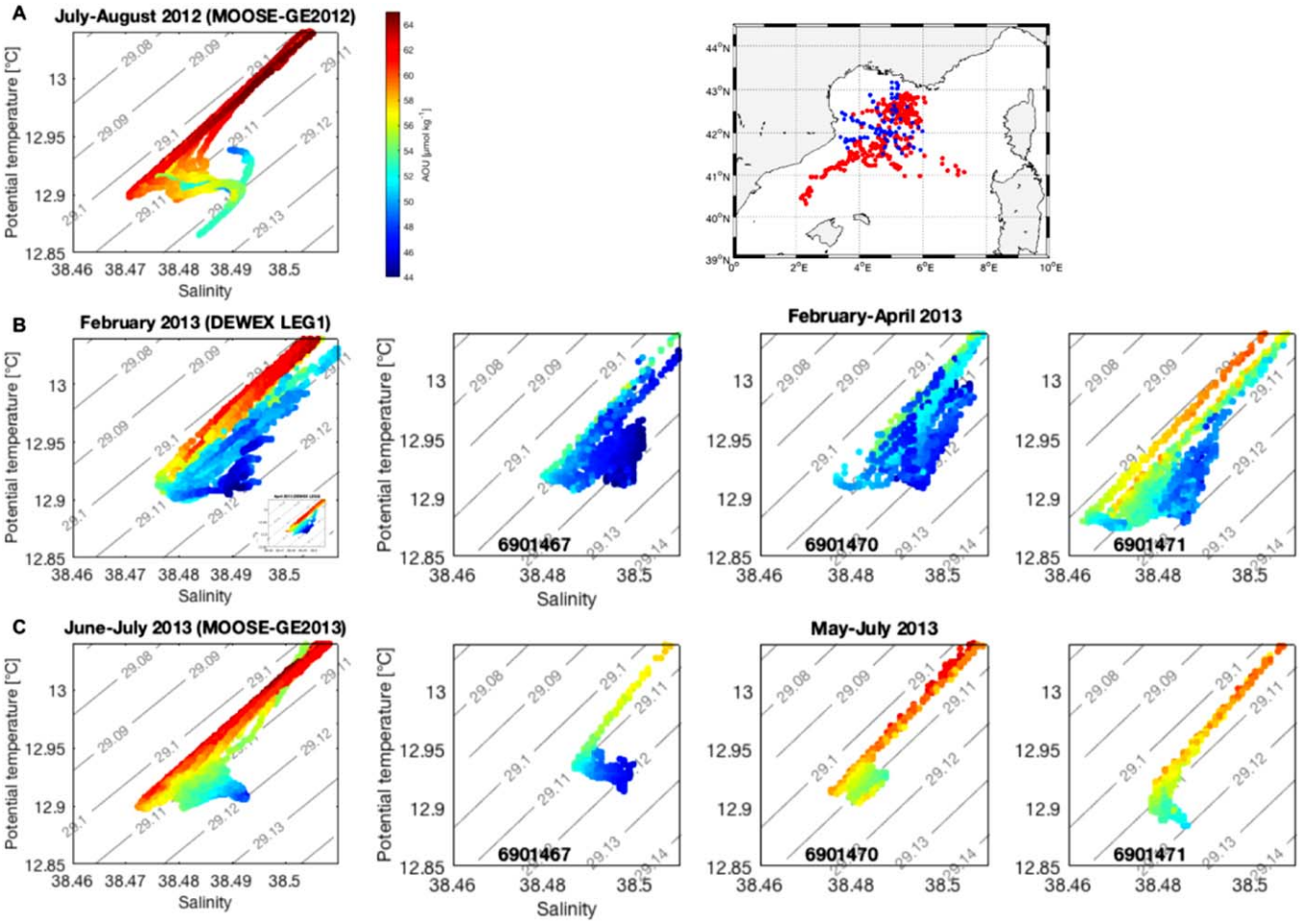


**Figure 6.** $\theta$-S diagrams for deep waters (WMDW) observed by shipborne CTD casts operated during the research cruises (left: MOOSE-GE2012, DEWEX, and MOOSE-GE2013) and by the three Argo floats (right: 6901467, 6901470, and 6901471) at different periods: (a) summer 2012 (before DWF), (b) winter-spring 2013 (during the DWF) and summer 2013 (after DWF). The color dots represent the AOU concentrations. All locations of profiles represented on diagrams are shown on the map (blue for cruises and red for floats). In Figure 6b, the inset represents the $\theta$-S diagram with AOU concentrations for deep waters in April 2013 (DEWEX LEG2).

casts, operated in summer 2012 in the north-western basin, a first hook from old dense waters is clearly visible on $\theta$-S diagram with AOU higher than 60 µmol kg$^{-1}$ (Figure 6a) which was probably formed during the 2005 event (WMT). During this event, LIW (warmer and saltier) and a long preconditioning period contributed to the formation of a new WMDW in the Gulf of Lion and in the Ligurian Sea, increasing rapidly temperature and salinity in deep waters [*Zunino et al.*, 2012]. The second hook in $\theta$-S diagram in 2012 is colder and fresher than the first hook and it shows lower AOU values (<56 µmol kg$^{-1}$), suggesting a more recent dense water formation. It could result from mixing between the two WMDW formed in 2005 and 2012 where cascading process (dense water formation from the shelf) provided colder and fresher dense waters into bottom waters [*Durrieu de Madron et al.*, 2013]. During the intense DWF event in February–March 2013, the water column is completely ventilated and lowest AOU (in deep blue on Figure 6b) appeared into the deep waters, which is consistent to rapid and intense deep $O_2$ supply. During this period, a decline of AOU below 48 µmol kg$^{-1}$ is clearly visible and related to the shift of $O_2$ concentrations in deep waters from 196 to 205 µmol kg$^{-1}$ (Table 2 and Figure 6b). Therefore, this sudden drop in AOU can be associated with the deep

**Table 2.** Estimation of the Dense Water Volume ($10^{13}$ m$^3$) From Argo-$O_2$ Floats and Ship Cruises (DEWEX and MOOSE-GE) During the Period 2012–2013[a]

| Period | Summer 2012 | Winter 2013[b] | Summer 2013 |
|---|---|---|---|
| AOU criteria (µmol kg$^{-1}$) | <56 | <48 | <52 |
| Dense water volume ($10^{13}$ m$^3$) | 0.15 | 1.50 | 0.20 |
| $O_2$ (µmol kg$^{-1}$) | 196 ± 1 | 205 ± 1 | 202 ± 2 |

[a]The volume has been estimated based on a AOU threshold and for potential density higher than 29.11 kg m$^{-3}$. The mean $O_2$ concentration observed in the dense water is also indicated.
[b]Period from January to April 2013.

ventilation process and representative to the upper limit of the newly formed dense waters, characterized by a potential density threshold of 29.11 kg $m^{-3}$ [*Waldman et al.*, 2016]. In April 2013, the newly formed WDMW shows still some low AOU values (DEWEX LEG2 cruise, Figure 6b), supporting the idea that the AOU threshold can be applied from January to April 2013. The subsequent summer, the Argo floats were located at southwest (6901467) and northeast of the DWF area (6901470 and 6901471) and observed different AOU concentrations. While the float 6901467 followed the spreading of the newly ventilated dense water (low AOU values in deep waters), the floats 6901470 and 6901471 observed deep waters faintly influenced by the dense water spreading (AOU values lower than 52 μmol $kg^{-1}$; Figure 6c). Based on this AOU evolution in deep waters from summer 2012 to summer 2013, we suggest to use the AOU concentration of 48 μmol $kg^{-1}$ and the typical potential density value (29 kg $m^{-3}$) for dense waters formation in the north-western basin as thresholds defining the apparition of new ventilated dense waters. Out of these limits, the dense waters might be result from deep mixing with older dense water (higher AOU concentrations) and it should not be taken into account in the volume calculation.

To check the robustness of this AOU threshold, the detection of dense water with AOU lower than 48 μmol $kg^{-1}$ observed by the three Argo floats is shown in Figure 7 and supporting information Figure S2. For float 6901467, the apparition of the AOU criterion in dense waters started from 15 February—after a strong Mistrals event—to the end of May. For the floats 6901470 and 6901471, we observed that the AOU criterion started from 7 February to end of March (Figure 7). These observations are consistent with the DWF 2013 process characterized by a peak of dense water production during the strong mistral event of 23–25 February (triggering the formation of dense water) followed by a period of restratification before a last event of bottom convection on 13–15 March [*Léger et al.*, 2016]. Moreover, it is essential to point out, that the AOU and density criteria were observed by the float 6901467 after a deep ML (Figure 7). This emphasizes the fact low AOU and dense waters were observed only after the first bottom reaching convection, which needed to be strong enough to mix a large volume of water in order to provide recent dense water mass into deep waters. Results shown in Figure 7 suggests also that the float 6901467 seems to follow postconvection spreading of the new ventilated water since the number of counts gradually reduces in time (consistent with low AOU values in deep waters; Figure 6c) while the floats 6901470 and 6901471 seem to leave the DWF zone in the end of March (they moved respectively to the north and to the east), which is consistent with the abrupt reduction of counts number. Consequently, the reduction of counts number in Figure 7 corresponds to shallower ML but also to an exit of floats from the DWF zone. Finally, these results indicate that AOU and density criteria are consistent with ventilation process into deep waters which is not only depending on the ML deepening but also on the newly formed dense water sinking. Indeed, the recent nature of the new ventilated dense waters suggests that vertical mixing should be strong and sustainable enough to sink rapidly the upper layer of oxygen-rich water into deep waters with low $O_2$ dispersion. In this case, the

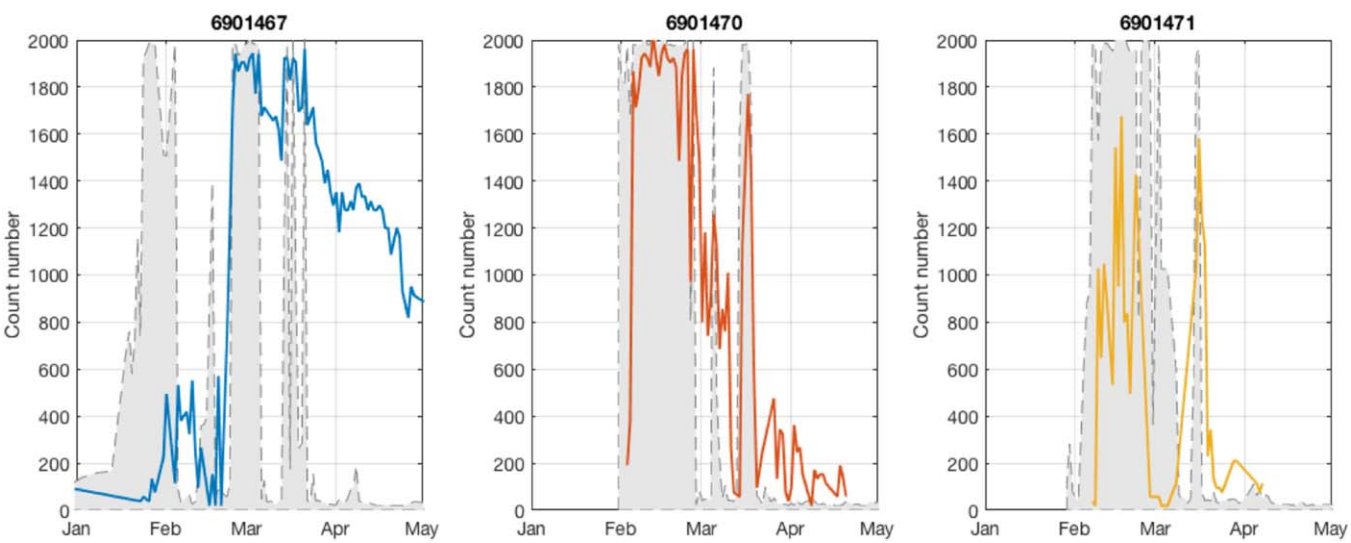


**Figure 7.** Evolution of count number of samples after interpolation for each meter of individual profile following the AOU and density thresholds (<48 μmol $kg^{-1}$ and >29.11 kg $m^{-3}$) for Argo floats 6901467 (blue), 6901470 (red), and 6901471 (yellow). The grey area in the background represents the ML depth observed by respective floats.

convective chimney, prevailing in the Gulf of Lion during DWF, is a key process to provide enough oxygen-rich content into deep layers compared to ML deepening which can be too short or too sporadic to modify the deep $O_2$ pool.

Based on the AOU and potential density thresholds in winter 2013 ($<$48 μmol kg$^{-1}$ and $>$29.11 kg m$^{-3}$, respectively), an interpolated surface was defined and representative to the upper depth boundary of the new ventilated dense water (see section 2.6). If we consider that this ventilated water supplied the deep layer down to the seafloor, the ventilated dense water volume was estimated to be about 1.5 $\times$ 10$^{13}$ m$^3$ during the DWF episode (January–April 2013; Table 2). This represents an exceptional convective event considering that the volume of the ventilated dense water during the previous and next summer (2012 and 2013) was much lower, about 0.15–0.2 $\times$ 10$^{13}$ m$^3$. Compared to models simulations, which estimated a dense water volume of 4 $\times$ 10$^{13}$ m$^3$ between winter 2012/2013 and spring 2013 [*Waldman et al*., 2016], our estimation is smaller. The difference is mainly due to our approach which is more focused on deep ventilation mechanism while models based their simulation only on potential density threshold (29.11 kg m$^{-3}$) and physical mixing. In addition, the DWF size area in models was higher than those observed by Argo floats during the convective event. Consequently, it is rather more judicious to compare both DWF rates (convected volume divided by the time period). From our approach, the deep ventilation rate is around 1.45 Sv and then close to *Waldman et al*. [2016] and *Estournel et al*. [2016] who simulated a DWF rate from summer 2012 to spring 2013 around 1.4 and 1.6 Sv, respectively.

Concerning the methodology used in the present study, it is important to underline that our approach is based on intense in situ profiles provided by Argo floats deployment during a convective episode whereas previous studies were based on simulation forced by in situ shipborne CTD casts with lower space-time resolution. Our methodology can be applied here thanks to daily vertical profiles acquisition and data adjustment operated in this study. Moreover, the AOU threshold allows to detect only the new ventilated dense water as older dense waters may have lost some $O_2$ concentrations by diffusion and/or bacterial activity (respiration). However, our method here depends on Argo floats space-time coverage and Argo floats depth limitation. For instance, Argo floats could sample several times the same ventilated dense water while missing other areas or they could miss some ventilated volume below 2000 m or they could visit the mixed patch outside the DWF period. At the same time, the assumption used in our approach supposes that the new ventilated volume supplies the deep layer until the seafloor. However, it could happen that during a less intense deep convection, the ventilation process would affect only the deep waters without any influence to the bottom layer. In this case, our approach would overestimate the new ventilated dense water. In the present study, the deep ventilation occurring in 2013 in the Gulf of Lion was intense enough to reach the seafloor [*Houpert et al*., 2016; Testor, personal communication, 2016] and then our method seems realistic enough to be applied here.

Estimating the volume and the rate of deep ventilation is essential to characterize the intensity of the DWF and its impact on deep marine ecosystem where consumption of $O_2$ by deep-dwelling organisms is critical [*Keeling et al*., 2010]. It allows to episodically renew the oxygen content in deep waters and to convey fresh organic matter that fuels the deep ecosystems [*Tamburini et al*., 2013]. Compared to previous convection events in the Gulf of Lion, the DWF 2013 is one of the most intense [*Houpert et al*., 2016; *Stabholz et al*., 2013]: it was higher than those observed in 2012 [*Durrieu de Madron et al*., 2013] but lower than those in 2005 [*Schroeder et al*., 2010]. In Figure 8, the representation of the spatial distribution of the new ventilated dense water volume reveals that a large quantity of ventilated water volume in winter 2013 was formed in the north-west part of the north-western basin. This is consistent with the results from SYMPHONIE model showing higher dense water thickness in the same area [*Waldman et al*., 2016] and previous studies using bottom potential density anomaly [*Durrieu de Madron et al*., 2013; *Estournel et al*., 2016]. The Gulf of Lion area is considered as the core of DWF for the north-western Mediterranean Sea due to the presence of dominant cold and dry winds (Mistrals and Tramontane) in winter, inducing loss of heat and densification of surface waters [*Durrieu de Madron et al*., 2013]. During the spreading of dense water, a large quantity of $O_2$ is ventilated into deep waters, moving to south and to the east. Such $O_2$ supply is consistent with previous deep $O_2$ concentrations increase observed in the western part of the Ligurian Sea from 2007 to 2010 and associated with open-sea convection events in the Gulf of Lion [*Tamburini et al*., 2013]. Consequently, the event in 2013 can be considered as exceptionally convective inducing an intense deep ventilation rate with possible impacts on organic carbon content and marine ecosystems in the Gulf of Lion and to a lesser extent in the Ligurian Sea by dense water spreading.

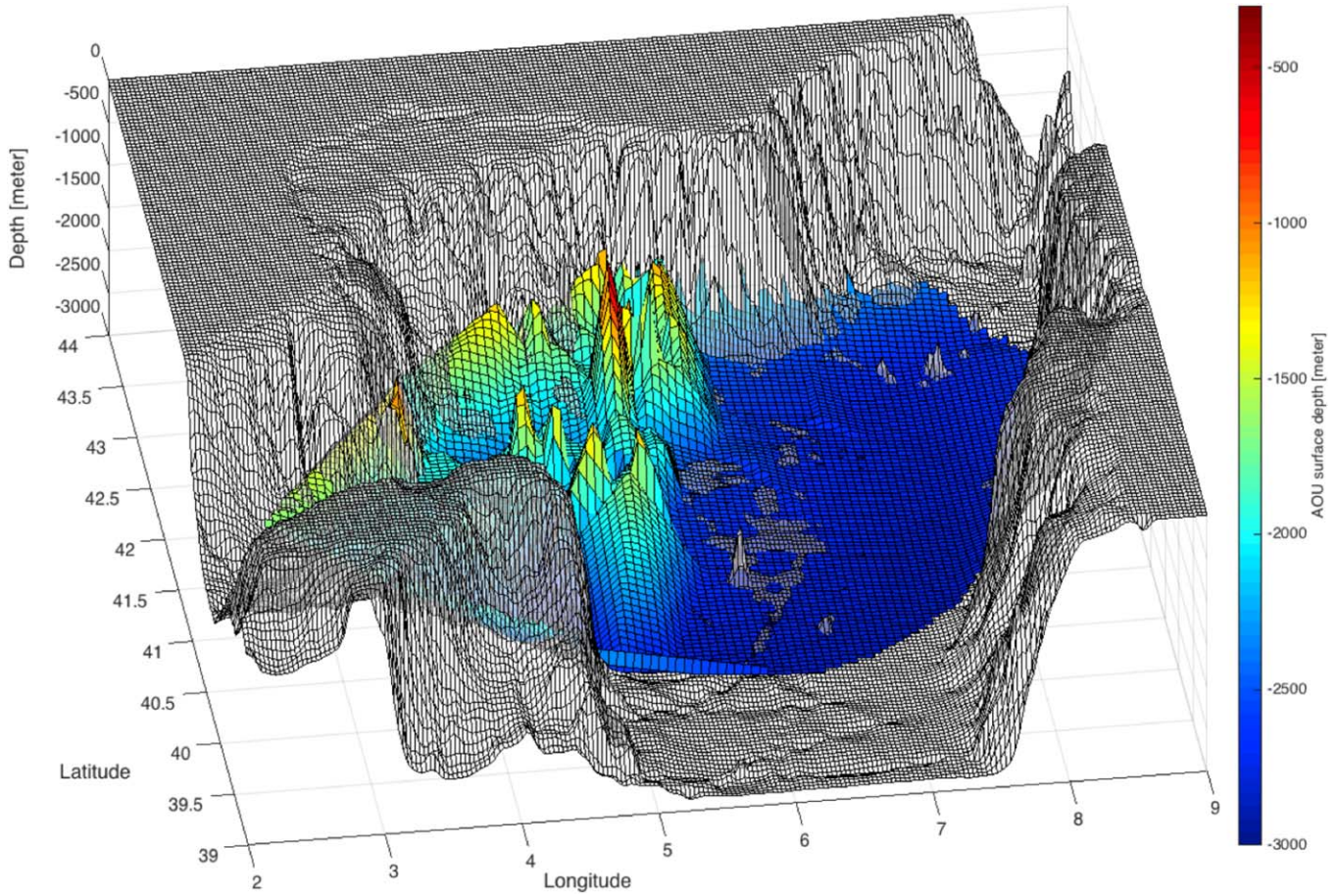


**Figure 8.** A 3-D view of the ventilated dense water volume located between the bottom depth and the minimum depth of the dense water mass within the AOU and potential density thresholds ($<$48 μmol kg$^{-1}$ and $>$29.11 kg m$^{-3}$, respectively) from January to April 2013. This estimation was done by merging Argo floats and shipborne CTD casts data (in total 287 profiles) and by using the Delaunay interpolation method (see section 2.6).

## 4. Conclusions

Intense deployment of Argo floats and regular cruises provided an important data set to quantify $O_2$ ventilation due to the open-sea convection in winter 2013 in the north-western Mediterranean basin. High space-time resolution and coverage of $O_2$ measurements suggest that the ML deepening influenced rapidly $O_2$ intake at rates higher than those observed in the Labrador Sea. During the DWF process, surface $O_2$ ingassing and outgassing seems to influence largely the $O_2$ inventory from January to March while biology activity occurring from April controls the $O_2$ inventory in the upper layer. Intense $O_2$ observation during the DWF event in 2013 provided an estimation of the volume of ventilated dense water recently formed in the Gulf of Lion based on AOU and potential density thresholds, typical of recent dense waters (48 μmol kg$^{-1}$ and 29.11 kg m$^{-3}$). While this approach benefits from intense Argo floats deployments to better parametrize the ventilated volume, the AOU threshold method probably underestimated the total ventilated volume inside the mixed patch. Nonetheless, it yielded precious information on ventilated dense water spreading and the $O_2$ supply affecting the deep waters in winter 2013, which can be still considered as an exceptionally convective event. Finally, our study suggests that new observational platforms and sensors could make $O_2$ a key parameter for addressing major issues of deep convection but also global change research during the 21st century.

**Acknowledgments**

This study is a contribution to the MerMex (Marine Ecosystem Response in the Mediterranean Experiment) and HyMeX (Hydrological cycle in the Mediterranean EXperiment) projects of the MISTRALS international program. The Argo floats and cruises data were collected and made freely available by the GDAC CORIOLIS (http://www.coriolis.eu.org) and SISMER database for French oceanographic cruises (http://www.ifremer.fr/sismer/). This work is a contribution to the ANR ASICS-MED project (grant ANR-12-BS06–0003). The authors are also grateful to the GMMC program that supported this work. Authors are also thankful to John Nolan (LOV, CNRS) for its review of the English text in our manuscript.

## References

Argo (2000), *Argo Float Data and Metadata From Global Data Assembly Centre (Argo GDAC)*, SEANOE, Brest, France, doi:10.17882/42182.

Benson, B. B., and D. Krause (1984), The concentration and isotopic fractionation of oxygen dissolved in freshwater and seawater in equilibrium with the atmosphere1, *Limnol. Oceanogr.*, *29*(3), 620–632, doi:10.4319/lo.1984.29.3.0620.

Béranger, K., Y. Drillet, M.-N. Houssais, P. Testor, R. Bourdallé-Badie, B. Alhammoud, A. Bozec, L. Mortier, P. Bouruet-Aubertot, and M. Crépon (2010), Impact of the spatial distribution of the atmospheric forcing on water mass formation in the Mediterranean Sea, *J. Geophys. Res.*, *115*, C12041, doi:10.1029/2009JC005648.

Bethoux, J. P. (1980), Mean water fluxes across sections in the Mediterranean-Sea, evaluated on the basis of water and salt budgets and of observed salinities, *Oceanol. Acta*, *3*(1), 79–88.

Bosse, A., P. Testor, L. Mortier, L. Prieur, V. Taillandier, F. d'Ortenzio, and L. Coppola (2015), Spreading of Levantine Intermediate Waters by submesoscale coherent vortices in the northwestern Mediterranean Sea as observed with gliders, *J. Geophys. Res. Oceans*, *120*, 1599–1622, doi:10.1002/2014JC010263.

Bosse, A., et al. (2016), Scales and dynamics of Submesoscale Coherent Vortices formed by deep convection in the northwestern Mediterranean Sea, *J. Geophys. Res. Oceans*, *121*, 7716–7742, doi:10.1002/2016JC012144.

CIESM (2009), Dynamics of Mediterranean deep waters, in *N° 38 in CIESM Workshop Monographs*, edited by F. Briand, p. 132, Monaco.

Conan, P. (2013), *DEWEX-MERMEX 2013 LEG2 cruise, RV Le Suroît*, SISMER, Brest, France, doi:10.17600/13020030.

Copin-Montégut, C., and M. Bégovic (2002), Distributions of carbonate properties and oxygen along the water column (0–2000 m) in the central part of the NW Mediterranean Sea (Dyfamed site): Influence of winter vertical mixing on air–sea $CO_2$ and $O_2$ exchanges, *Deep Sea Res., Part II*, *49*(11), 2049–2066, doi:10.1016/s0967-0645(02)00027-9.

D'Ortenzio, F., D. Ludicone, C. de Boyer Montegut, P. Testor, D. Antoine, S. Marullo, R. Santoleri, and G. Madec (2005), Seasonal variability of the mixed layer depth in the Mediterranean Sea as derived from in situ profiles, *Geophys. Res. Lett.*, *32*, L12605, doi:10.1029/2005GL022463.

Durrieu de Madron, X., et al. (2013), Interaction of dense shelf water cascading and open-sea convection in the northwestern Mediterranean during winter 2012, *Geophys. Res. Lett.*, *40*, 1379–1385, doi:10.1002/grl.50331.

Estournel, C., et al. (2016), High resolution modeling of dense water formation in the north-western Mediterranean during winter 2012–2013: Processes and budget, *J. Geophys. Res. Oceans*, *121*, 5367–5392, doi:10.1002/2016JC011935.

Frob, F., A. Olsen, K. Vage, G. W. Moore, I. Yashayaev, E. Jeansson, and B. Rajasakaren (2016), Irminger Sea deep convection injects oxygen and anthropogenic carbon to the ocean interior, *Nat. Commun.*, *7*, 13244, doi:10.1038/ncomms13244.

Garcia, H. E., and L. I. Gordon (1992), Oxygen solubility in seawater: Better fitting equations, *Limnol. Oceanogr.*, *37*(6), 1307–1312, doi:10.4319/lo.1992.37.6.1307.

Herrmann, M., S. Somot, F. Sevault, C. Estournel, and M. Déqué (2008), Modeling the deep convection in the northwestern Mediterranean Sea using an eddy-permitting and an eddy-resolving model: Case study of winter 1986–1987, *J. Geophys. Res.*, *113*, C04011, doi:10.1029/2006JC003991.

Herrmann, M., F. Sevault, J. Beuvier, and S. Somot (2010), What induced the exceptional 2005 convection event in the northwestern Mediterranean basin? Answers from a modeling study, *J. Geophys. Res.*, *115*, C12051, doi:10.1029/2010JC006162.

Houpert, L., et al. (2016), Observations of open-ocean deep convection in the northwestern Mediterranean Sea: Seasonal and interannual variability of mixing and deep water masses for the 2007–2013 Period, *J. Geophys. Res. Oceans*, *121*, 8139–8171, doi:10.1002/2016JC011857.

Ito, T., M. J. Follows, and E. A. Boyle (2004), Is AOU a good measure of respiration in the oceans?, *Geophys. Res. Lett.*, *31*, L17305, doi:10.1029/2004GL020900.

Keeling, R. E., A. Kortzinger, and N. Gruber (2010), Ocean deoxygenation in a warming world, *Annu. Rev. Mar. Sci.*, *2*, 199–229, doi:10.1146/annurev.marine.010908.163855.

Kortzinger, A., J. Schimanski, U. Send, and D. Wallace (2004), The ocean takes a deep breath, *Science*, *306*(5700), 1337, doi:10.1126/science.1102557.

Leaman, K. D., and F. A. Schott (1991), Hydrographic structure of the convection regime in the Gulf of Lions: Winter 1987, *J. Phys. Oceanogr.*, *21*(4), 575–598.

Léger, F., C. Lebeaupin Brossier, H. Giordani, T. Arsouze, J. Beuvier, M.-N. Bouin, É. Bresson, V. Ducrocq, N. Fourrié, and M. Nuret (2016), Dense water formation in the north-western Mediterranean area during HyMeX-SOP2 in 1/36° ocean simulations: Sensitivity to initial conditions, *J. Geophys. Res. Oceans*, *121*, 5549–5569, doi:10.1002/2015JC011542.

López-Jurado, J. L., C. González-Pola, and P. Vélez-Belchí (2005), Observation of an abrupt disruption of the long-term warming trend at the Balearic Sea, western Mediterranean Sea, in summer 2005, *Geophys. Res. Lett.*, *32*, L24606, doi:10.1029/2005GL024430.

Loveday, B. R., S. Swart, and D. Storkey (2012), Capturing convection in the northwest Mediterranean Sea: Using underwater gliders to assess the performance of regional forecast models, *Underwater Technol.*, *30*(3), 135–149, doi:10.3723/ut.30.135.

Marshall, J., and F. Schott (1999), Open-ocean convection: Observations, theory, and models, *Rev. Geophys.*, *37*(1), 1–64, doi:10.1029/98RG02739.

Mayot, N., F. D'Ortenzio, V. Taillandier, L. Prieur, O. Pasqueron de Fommervault, H. Claustre, A. Bosse, P. Testor, and P. Conan (2017), Physical and biogeochemical controls of the phytoplankton blooms in north-western Mediterranean Sea: A multiplatform approach over a complete annual cycle (2012–2013 DEWEX experiment), *J. Geophys. Res. Oceans*, *122*, doi:10.1002/2016JC012052, in press.

Millot, C., and I. Taupier-Letage (2005), Circulation in the Mediterranean Sea, in *The Mediterranean Sea, Handbook of Environmental Chemistry*, edited by A. Saliot, vol. 5K, Springer, Berlin, Heidelberg.

Rhein, M. (1995), Deep water formation in the western Mediterranean, *J. Geophys. Res.*, *100*(C4), 6943, doi:10.1029/94JC03198.

Schneider, A., T. Tanhua, W. Roether, and R. Steinfeldt (2014), Changes in ventilation of the Mediterranean Sea during the past 25 year, *Ocean Sci.*, *10*(1), 1–16, doi:10.5194/os-10-1-2014.

Schroeder, K., M. Borghini, G. Cerrati, V. Difesca, R. Delfanti, C. Santinelli, and G. P. Gasparini (2008a), Multiparametric mixing analysis of the deep waters in the Western Mediterranean Sea, *Chem. Ecol.*, *24*, suppl. 1, 47–56, doi:10.1080/02757540801970373.

Schroeder, K., A. Ribotti, M. Borghini, R. Sorgente, A. Perilli, and G. P. Gasparini (2008b), An extensive western Mediterranean deep water renewal between 2004 and 2006, *Geophys. Res. Lett.*, *35*, L18605, doi:10.1029/2008GL035146.

Schroeder, K., S. A. Josey, M. Herrmann, L. Grignon, G. P. Gasparini, and H. L. Bryden (2010), Abrupt warming and salting of the Western Mediterranean Deep Water after 2005: Atmospheric forcings and lateral advection, *J. Geophys. Res.*, *115*, C08029, doi:10.1029/2009JC005749.

Schroeder, K., T. Tanhua, H. Bryden, M. Alvarez, J. Chiggiato, and S. Aracri (2015), Mediterranean Sea Ship-based Hydrographic Investigations Program (Med-SHIP), *Oceanography*, *28*(3), 12–15, doi:10.5670/oceanog.2015.71.

Stabholz, M., et al. (2013), Impact of open-ocean convection on particle fluxes and sediment dynamics in the deep margin of the Gulf of Lions, *Biogeosciences*, *10*(2), 1097–1116, doi:10.5194/bg-10-1097-2013.

Stöven, T., and T. Tanhua (2014), Ventilation of the Mediterranean Sea constrained by multiple transient tracer measurements, *Ocean Sci.*, *10*(3), 439–457, doi:10.5194/os-10-439-2014.

Taillandier, V., A. Griffa, P. M. Poulain, and K. Béranger (2006), Assimilation of Argo float positions in the north western Mediterranean Sea and impact on ocean circulation simulations, *Geophys. Res. Lett.*, *33*, L11604, doi:10.1029/2005GL025552.
Takeshita, Y., T. R. Martz, K. S. Johnson, J. N. Plant, D. Gilbert, S. C. Riser, C. Neill, and B. Tilbrook (2013), A climatology-based quality control procedure for profiling float oxygen data, *J. Geophys. Res. Oceans*, *118*, 5640–5650, doi:10.1002/jgrc.20399.
Tamburini, C., et al. (2013), Deep-sea bioluminescence blooms after dense water formation at the ocean surface, *PLoS One*, *8*(7), e67523, doi:10.1371/journal.pone.0067523.
Taupier-Letage, I., and C. Bachelier (2013), CTD_SOP2, Provence - Tethys 2, SEDOO, OMP, Toulouse, doi:10.6096/MISTRALS-HyMeX.950.
Testor, P. (2013), *DEWEX-MERMEX 2013 LEG1 cruise, RV Le Suroit*, SISMER, Brest, France, doi:10.17600/13020010.
Testor, P., and J. C. Gascard (2006), Post-convection spreading phase in the Northwestern Mediterranean Sea, *Deep Sea Res., Part I*, *53*(5), 869–893, doi:10.1016/j.dsr.2006.02.004.
Testor, P., L. Coppola, and L. Mortier (2012), *MOOSE-GE 2012 cruise, R/V Le Suroit*, SISMER, Brest, France, doi:10.17600/12020030.
Testor, P., L. Coppola, and L. Mortier (2013), *MOOSE-GE 2013 cruise, RV Téthys II*, SISMER, Brest, France, doi:10.17600/13450110.
Thierry, V., and H. Bittig, and Argo-Team (2016), *Argo Quality Control Manual for Dissolved Oxygen Concentration*, doi:10.13155/46542.
Uchida, H., T. Kawano, I. Kaneko, and M. Fukasawa (2008), In situ calibration of optode-based oxygen sensors, *J. Atmos. Oceanic Technol.*, *25*(12), 2271–2281, doi:10.1175/2008JTECHO549.1.
Waldman, R., et al. (2016), Estimating dense water volume and its evolution for the year 2012–2013 in the Northwestern Mediterranean Sea: An observing system simulation experiment approach, *J. Geophys. Res. Oceans*, *121*, 6696–6716, doi:10.1002/2016JC011694.
Zunino, P., K. Schroeder, M. Vargas-Yáñez, G. P. Gasparini, L. Coppola, M. C. García-Martínez, and F. Moya-Ruiz (2012), Effects of the Western Mediterranean Transition on the resident water masses: Pure warming, pure freshening and pure heaving, *J. Mar. Syst.*, *96–97*, 15–23, doi:10.1016/j.jmarsys.2012.01.011.

Supporting Information for

# Observation of oxygen ventilation into deep waters through targeted deployment of multiple Argo-O2 floats in the north western Mediterranean Sea in 2013

L. Coppola[1], L. Prieur[1], I. Taupier-Letage[2], C. Estournel[3], P. Testor[4], D. Lefevre[2], S. Belamari[5], S. LeReste[6], V. Taillandier[1]

[1]Sorbonne Universités, UPMC, Université Paris 06, CNRS, Laboratoire d'Océanographie de Villefranche, 181 Chemin du Lazaret, 06230 Villefranche-sur-Mer, France

[2]Aix-Marseille Université, CNRS/INSU, Université de Toulon, IRD, Mediterranean Institute of Oceanography (MIO), UM 110, 13288 Marseille Cedex 9, France

Mediterranean Institute of Oceanography (MIO), 13288 Marseille Cedex 9, France

[3]Université de Toulouse, CNRS, Laboratoire d'Aérologie, Toulouse, France

[4]CNRS/IRD/UPMC University Paris 06, MNHN, LOCEAN, Paris, France

[5]Météo-France, CNRS, CNRM-GAME, Toulouse, France

[6]IFREMER RDT/I2M, Brest, France

## Contents of this file



## Additional Supporting Information (Files uploaded separately)

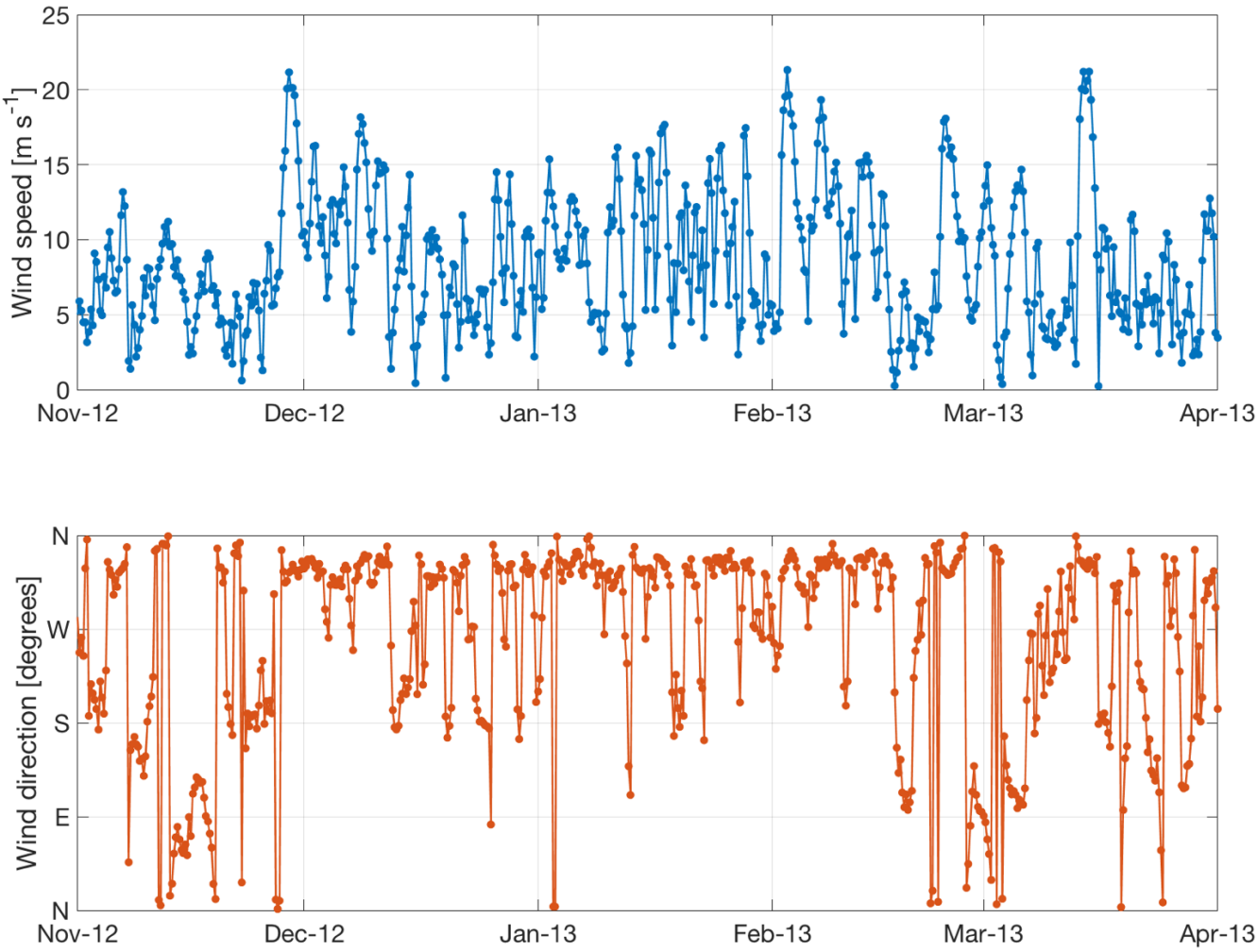


**Figure S1.** Wind speed and direction time series at 10 m from November 2012 to April 2013. 6-hourly wind data are extracted from ECMWF (European Centre for Medium-Range Weather Forecasts) re-analysis at the LION buoy location (42.1°N-4.7°E). Wind direction is reported in cardinal directions (measured in degrees clockwise from due north).

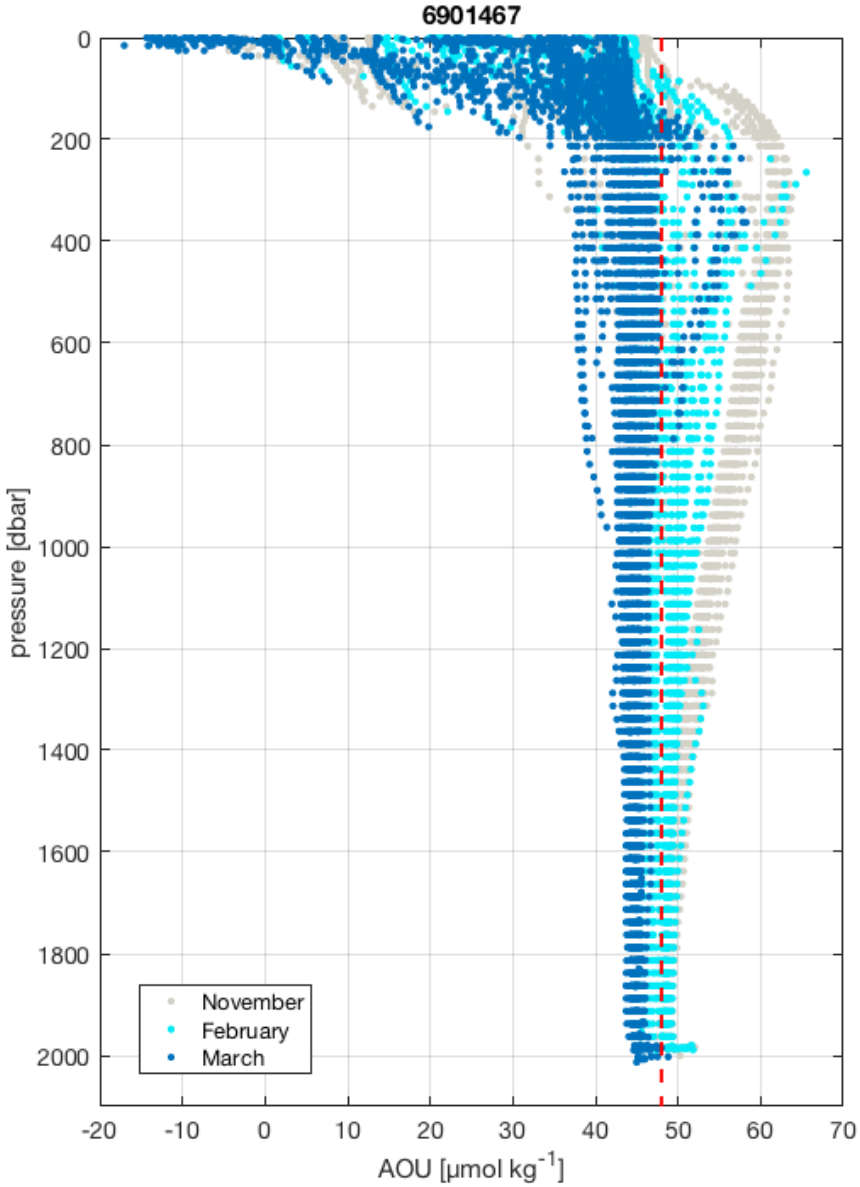


**Figure S2**. Apparent Oxygen Utilization (AOU) vertical profiles (in µmol $kg^{-1}$) for Argo float 6901467 at different periods: November (grey), February (dark blue) and March (light blue). The red dashed line represents the AOU threshold (48 µmol $kg^{-1}$).